

Emergence of rheological properties in lattice Boltzmann simulations of gyroid mesophases

G. GIUPPONI¹, J. HARTING² and P.V. COVENEY¹

¹ *Centre for Computational Science, Department of Chemistry, University College London - 20, Gordon Street, WC1H 0AJ, London, UK*

² *Institute for Computational Physics, University of Stuttgart - Pfaffenwaldring 27, 70569 Stuttgart, Germany*

PACS. 47.11.+j – Computational methods in fluid dynamics.

PACS. 82.70.Uv – Surfactants, micellar solutions, vesicles, lamellae, amphiphilic systems, (hydrophilic and hydrophobic interactions).

PACS. 83.60.-a – Rheology, Material behaviour.

Abstract. – We use a lattice Boltzmann (LB) kinetic scheme for modelling amphiphilic fluids that correctly predicts rheological effects in flow. No macroscopic parameters are included in the model. Instead, three-dimensional hydrodynamic and rheological effects are emergent from the underlying particulate conservation laws and interactions. We report evidence of shear thinning and viscoelastic flow for a self-assembled gyroid mesophase. This purely kinetic approach is of general importance for the modelling and simulation of complex fluid flows in situations when rheological properties cannot be predicted *a priori*.

Introduction. – Lattice Boltzmann (LB) modelling schemes have emerged in the last several years as a powerful approach for simulating the dynamics of a variety of complex systems, from flow with suspended particles to multiphase flow through porous media [1]. Of great interest is the extension of this method to the modelling of flow properties of viscoelastic materials such as polymer melts and amphiphilic fluids, where the dynamics of microscopic structures is coupled to the flow.

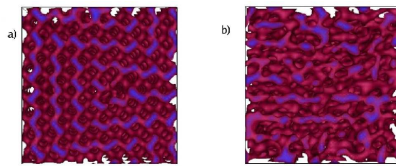


Fig. 1 – a) High-density volume rendering of one of the two immiscible fluids (red) and interface between the two (blue) in the gyroid mesophase. b) Same as in a), but after 8000 simulation timesteps with an imposed steady shear ($U = 0.1, \omega = 0$ in eq. (6)). The shear reduces the crystallinity and the material assumes more fluid-like properties. Model size is 64^3

Qian and Deng [2] correctly described transverse wave propagation using a lattice BGK model with an *ad hoc* modified equilibrium distribution while Ispolatov and Grant [3] obtained viscoelastic effects by adding a force to represent memory effects in the LB equation. However, both approaches involve the inclusion of macroscopic parameters such as Young's modulus [2] or elastic coefficients [3]. These methods cannot be regarded as fully mesoscopic as at least one parameter is imposed on the basis of macroscopic considerations. Giraud et al. [4] introduced a single fluid, two dimensional model to treat a macroscopically viscoelastic fluid and later Lallemand et al. [5] extended this model to three dimensions, but to the best of our knowledge no generalization for multiphase flow or flow with suspended particles has yet been implemented. A free energy Ginzburg-Landau (GL) model can be defined to study rheological properties of complex fluids [6,7]. A popular LB scheme based on the same GL approach proceeds by defining an equilibrium distribution through the imposition of constraints on macroscopic thermomechanical quantities such as the stress tensor. Using such a scheme, Denniston et al. [8] obtained non-Newtonian flow behaviour (including shear thinning and banding) using an LB algorithm for the hydrodynamics of liquid crystals in the isotropic and nematic phases. However, with such methods the dynamics is not dictated by the mesoscopic processes; numerical instability [9] can make this approach unsuitable for a fully mesoscopic description of the dynamics.

González and Coveney [10], using a fully mesoscopic, kinetic approach which does not require the existence of a thermodynamic potential obtained a self assembled gyroid mesophase in the course of simulating an amphiphilic fluid formed by two immiscible fluids and a surfactant species (fig. 1). The term amphiphilic fluid is used to describe a fluid in which at least one species is made of surfactant molecules. Surfactants are molecules comprised of a hydrophilic (water-loving) head group and a hydrophobic (oil-loving) tail. An amphiphilic fluid may contain oil, water, or both fluids in addition to surfactant. Such complex fluids can self-assemble to form ordered structures such as lamellae, micelles, sponge and liquid crystalline (cubic) phases showing pronounced rheological properties [11].

In this letter we use this purely kinetic LB method to model complex flows whose rheological properties are emergent from the mesoscopic kinetic processes without any imposed macroscopic constraints [12]. In particular, we show evidence of the appearance of rheological effects, such as shear thinning and viscoelasticity, for a self-assembled gyroid liquid crystalline cubic mesophase.

The model. – A standard LB system involving multiple species is usually represented by a set of equations [13]

$$n_i^\alpha(\mathbf{x} + \mathbf{c}_i, t + 1) - n_i^\alpha(\mathbf{x}, t) = -\frac{1}{\tau_\alpha}(n_i^\alpha(\mathbf{x}, t) - n_i^{\alpha eq}(\mathbf{x}, t)), \quad i = 0, 1, \dots, b, \quad (1)$$

where $n_i^\alpha(\mathbf{x}, t)$ is the single-particle distribution function, indicating the density of species α (for example, oil, water or amphiphile), having velocity \mathbf{c}_i , at site \mathbf{x} on a D-dimensional lattice of coordination number b , at time-step t . The collision operator Ω_i^α represents the change in the single-particle distribution function due to the collisions. We choose a single relaxation time τ_α , 'BGK' form [14] for the collision operator. In the limit of low Mach numbers, the LB equations correspond to a solution of the Navier-Stokes equation for isothermal, quasi-incompressible fluid flow whose implementation can efficiently exploit parallel computers, as the dynamics at a point requires only information about quantities at nearest neighbour lattice sites. The local equilibrium distribution $n_i^{\alpha eq}$ plays a fundamental role in the dynamics of the system as shown by eq. (1). In this study, we use a purely kinetic approach, for which the local equilibrium distribution $n_i^{\alpha eq}(\mathbf{x}, t)$ is derived by imposing certain restrictions on the

microscopic processes, such as explicit mass and total momentum conservation [15]

$$n_i^{\alpha eq} = \zeta_i n^\alpha \left[1 + \frac{\mathbf{c}_i \cdot \mathbf{u}}{c_s^2} + \frac{(\mathbf{c}_i \cdot \mathbf{u})^2}{2c_s^4} - \frac{u^2}{2c_s^2} + \frac{(\mathbf{c}_i \cdot \mathbf{u})^3}{6c_s^6} - \frac{u^2(\mathbf{c}_i \cdot \mathbf{u})}{2c_s^4} \right], \quad (2)$$

where $\mathbf{u} = \mathbf{u}(\mathbf{x}, t)$ is the macroscopic bulk velocity of the fluid, defined as $n^\alpha(\mathbf{x}, t)\mathbf{u}^\alpha \equiv \sum_i n_i^\alpha(\mathbf{x}, t)\mathbf{c}_i$, ζ_i are the coefficients resulting from the velocity space discretization and c_s is the speed of sound, both of which are determined by the choice of the lattice, which is D3Q19 in our implementation. Immiscibility of species α is introduced in the model following Shan and Chen [16, 17]. Only nearest neighbour interactions among the immiscible species are considered. These interactions are modelled as a self-consistently generated mean field body force

$$\mathbf{F}^\alpha(\mathbf{x}, t) \equiv -\psi^\alpha(\mathbf{x}, t) \sum_{\bar{\alpha}} g_{\alpha\bar{\alpha}} \sum_{\mathbf{x}'} \psi^{\bar{\alpha}}(\mathbf{x}', t)(\mathbf{x}' - \mathbf{x}), \quad (3)$$

where $\psi^\alpha(\mathbf{x}, t)$ is the so-called effective mass, which can have a general form for modelling various types of fluids (we use $\psi^\alpha = (1 - e^{-n^\alpha})$ [16]), and $g_{\alpha\bar{\alpha}}$ is a force coupling constant whose magnitude controls the strength of the interaction between components α , $\bar{\alpha}$ and is set positive to mimic repulsion. The dynamical effect of the force is realized in the BGK collision operator in eq. (??) by adding to the velocity \mathbf{u} in the equilibrium distribution of eq. (2) an increment

$$\delta\mathbf{u}^\alpha = \frac{\tau^\alpha \mathbf{F}^\alpha}{n^\alpha}. \quad (4)$$

As described above, an amphiphile usually possesses two different fragments, each having an affinity for one of the two immiscible components. The addition of an amphiphile is implemented as in [12]. An average dipole vector $\mathbf{d}(\mathbf{x}, t)$ is introduced at each site \mathbf{x} to represent the orientation of any amphiphile present there. The direction of this dipole vector is allowed to vary continuously and no information is specified for each velocity \mathbf{c}_i , for reasons of computational efficiency and simplicity. Full details of the model can be found in [12] and [18].

Simulation details. – We use LB3D [19], a highly scalable parallel LB code, to implement the model. A single simulation of a 64^3 model, i.e. a point in fig.2 below, needs around 300 Mbytes of RAM and takes about 50 CPU hours to complete on a single processor machine. The very good scaling of our LB3D code permits us to run all our simulations on multiprocessor machines and computational grids in order to reduce the length of data collection to a few weeks. The simulation parameters are those used in [10] that lead to the formation of gyroid mesophases. We use a 64^3 lattice size with periodic boundary conditions. The simulations were all started from a checkpointed configuration of a 200000 timesteps equilibrated gyroid mesophase [19]. A single unit cell of the gyroid minimal surface is of the order of 5 – 8 lattice lengths in its linear dimensions. This implies that hundreds of unit cells are present in a 64^3 sample. Therefore, finite size effects are not expected to affect the qualitative outcome of the simulations. Moreover, some simulations with a 128^3 lattice have been run to confirm the results obtained and the 128^3 simulations reported in [20] are consistent with the results shown here. Nevertheless, such lattice sizes oblige us to study perfect gyroids; much larger system sizes (and computational cost) would be necessary in order to investigate the role of domains and their associated defects [21]. We leave this for future work.

In order to inspect the rheological behaviour of gyroid mesophases, we have implemented Lees-Edwards boundary conditions, which reduce finite size effects if compared to moving solid

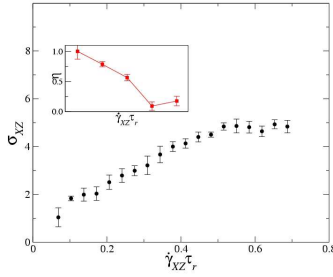


Fig. 2

Fig. 2 – Plot of σ_{xz} (dimensionless units) vs. shear rate $\dot{\gamma}_{xz}\tau_r$ (Weissenberg number) for an LB simulation of a 64^3 gyroid mesophase. τ_r is the stress relaxation time; see text for discussion. The inset shows the percentage drop of the viscosity as the shear rate $\dot{\gamma}_{xz}\tau_r$ increases (shear-thinning).

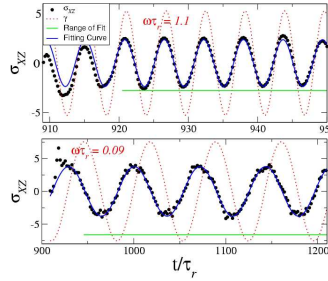


Fig. 3

Fig. 3 – Plot of σ_{xz} (black dots) vs. time for oscillatory shear ($U = 0.05$ and $\omega = 0.0004, 0.005$ in eq. (6)) applied to 64^3 lattice-Boltzmann gyroid mesophase. All quantities are dimensionless. After a brief transient, σ_{xz} oscillates with the imposed frequency $\omega\tau_r$. The strain (dashed line) is plotted (scaled) as a guide to the eye. The continuous line is the best fit line for the σ_{xz} data. Shear moduli $G'(\omega\tau_r)$, $G''(\omega\tau_r)$ are calculated as in eq. (9) over a time interval shown by the continuous horizontal line.

walls [22]. This computationally convenient method imposes new positions and velocities on particles leaving the simulation box in the direction perpendicular to the imposed shear strain while leaving the other coordinates unchanged. Choosing z as the direction of shear and x as the direction of the velocity gradient, we have

$$z' \equiv \begin{cases} (z + \Delta_z) \bmod N_z & , x > N_x \\ z \bmod N_z & , 0 \leq x \leq N_x \\ (z - \Delta_z) \bmod N_z & , x < 0 \end{cases} \quad u'_z \equiv \begin{cases} u_z + U & , x > N_x \\ u_z & , 0 \leq x \leq N_x \\ u_z - U & , x < 0 \end{cases} , \quad (5)$$

where $\Delta_z \equiv U\Delta t$, U is the shear velocity, u_z is the z -component of \mathbf{u} and $N_{x(z)}$ is the system length in the $x(z)$ direction. We also use an interpolation scheme suggested by Wagner and Pagonabarraga [23] as Δ_z is not generally a multiple of the lattice site. Cates et al. [24], found pronounced artefacts (lock-ins) in simulations of 2D sheared binary mixtures with multiple Lees-Edwards planes. In our own work, we have not seen any of these artefacts, even in the longest simulations performed, and a linear velocity profile is obtained at steady state.

Consistent with the hypothesis of the LB model, we set the maximum shear velocity to $U = 0.1$ lattice units. This results in a maximum shear rate $\dot{\gamma}_{xz} = \frac{2 \times 0.1}{64} = 3.2 \times 10^{-3}$ in lattice units. Simulations are run for $T = 10000$ timesteps in the case of steady shear. Steady state is reached in the first 1000 timesteps, and the relevant component of the stress tensor is averaged over the last 3000 timesteps. Some measurements were repeated by doubling the simulation time to a total of $T = 20000$ timesteps but no significant differences were found. For oscillatory shear, we set

$$U(t) = U \cos(\omega t) , \quad (6)$$

where $\omega/2\pi$ is the frequency of oscillation and $U = 0.05$ lattice units. These simulations were run for at least three complete oscillations, $t = 5000 - 100000$ timesteps.

Results. – In order to investigate rheological properties of the system, we perform simulations of flow under shear, mimicking a rheometer. We set $U = n \times 0.005$, $n = 2 \dots 21$ and

$\omega = 0$ to impose a stationary Couette flow. Once steady state flow is reached, we collect the relevant component of the pressure tensor σ_{xz} . According to Newton's law for viscous flow of a liquid we have

$$\sigma_{xz} = 2\eta\dot{\gamma}_{xz} , \quad (7)$$

where η is the viscosity of the liquid and $\dot{\gamma}_{xz} = \frac{(\partial_x u_z + \partial_z u_x)}{2}$. In fig. 2 we plot σ_{xz} against the imposed non-dimensionalized (see text below) shear rate $\dot{\gamma}_{xz}\tau_r$ (Weissenberg number). We note that the slope of the curve changes as these shear rate increases. This indicates that the viscosity η depends on the shear rate $\dot{\gamma}_{xz}$, $\eta = \eta(\dot{\gamma}_{xz})$. We therefore conclude that our model exhibits non-Newtonian flow behaviour. Complex fluids such as amphiphilic mixtures are well known to exhibit such behaviour experimentally [11]. In the inset we calculate the percentage drop of η by averaging the slope of the curve over subsets of four data points. We note that the viscosity decreases as the shear rate increases. This behaviour is referred to as ‘‘shear thinning’’ [11]. In general, fluids exhibit macroscopic non-Newtonian properties because of underlying complex mesoscopic interactions and leading to changes in their microstructural properties. In our case, the highly ordered structure of the gyroid mesophase is responsible for this rheological effect, and our LB model correctly captures it. Therefore, considering the underlying physics of mesophases, this simulation result is not only justified but also expected. We note that the predictions of the model could be directly verified, but no experimental evidence for gyroid rheology is currently available in the literature.

For oscillatory shear, in eq. (6) we set $U = 0.05$ lattice units and we span a range of two decades of frequencies by varying ω between $\omega = 0.0001$ and $\omega = 0.01$ lattice units. For a viscoelastic medium

$$\sigma_{xz} = \gamma_0[G'(\omega)\sin(\omega t) + G''(\omega)\cos(\omega t)] , \quad (8)$$

where $\gamma_0 = \frac{2U}{64\omega}$ is the imposed shear strain and $G'(\omega)$, $G''(\omega)$ are, respectively, the storage and loss moduli which respectively measure the elastic and viscous response at any given frequency [11]. In fig. 3 we show the time dependence of σ_{xz} for two simulations with different values of ω . After a brief transient, σ_{xz} begins to oscillate as predicted by eq. (8) with the imposed frequency ω and an amplitude σ_0 and shift ϕ that depend on the storage and loss moduli

$$G' = \frac{\sigma_0 \cos(\phi)}{\gamma} \quad G'' = \frac{\sigma_0 \sin(\phi)}{\gamma} , \quad (9)$$

where σ_0 and ϕ are the fitted values for the amplitude and phase shift. We derive $G'(\omega)$ and $G''(\omega)$ for the two different values of $\omega = 0.005, 0.0004$ by fitting σ_0 and ϕ with the standard Levenberg-Marquardt algorithm over at least three decades (see caption for details). In fig. 4, we plot σ_{xz} against the shear strain at different times (Lissajous plots) for the two frequencies of fig.3. We note that for the higher frequency (left panel), σ_{xz} is in phase with the strain, indicating that the gyroid mesophase exhibits a solid-like response at short timescales. For the smaller frequency, the phase shift is almost $\pi/2$, typical of a liquid-like response as dictated by eq. (7). In fig. 5, we plot $G'(\omega\tau_r)$ and $G''(\omega\tau_r)$ for the different simulation values of ω . In order to capture the relevant scales in the model, all quantities are dimensionless. In particular, the frequency ω has been multiplied by the characteristic stress relaxation time, $\tau_r \sim 220$ simulation timesteps, calculated by fitting the exponential decay of σ_{xz} when shear is removed. We note that a crossover between $G'(\omega\tau_r)$ and $G''(\omega\tau_r)$ occurs at $\omega\tau_r \sim 0.05$. This signals a transition between solid and liquid-like behaviour and indicates

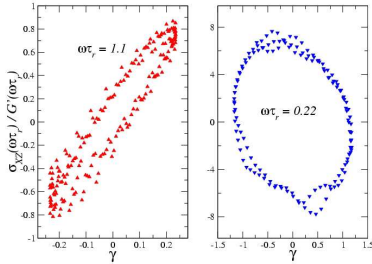


Fig. 4

Fig. 4 – Lissajous plots of σ_{xz} (in lattice units) vs. dimensionless strain γ_{xz} . In the left(right) panel, points tend to form a straight line (ellipse, respectively). This indicates that the pressure σ_{xz} is in(out) of phase with respect to the strain γ_{xz} , as typical for solid(liquid)-like phases. The overall behaviour is typical of viscoelastic fluids.

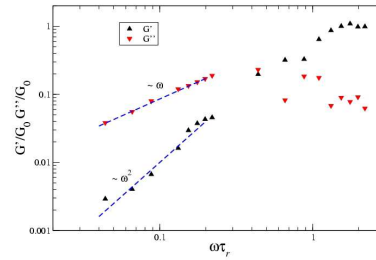


Fig. 5

Fig. 5 – Plots of shear moduli $G'(\omega\tau_r)$ (regular triangles), $G''(\omega\tau_r)$ (inverted triangles) calculated for all frequencies used in our simulations. We note that a crossover between liquid and solid-like behaviour occurs around $\omega = 0.5$. Theoretically, $G' \sim \omega^2$, $G'' \sim \omega$ as ω goes to 0. Our data agree with this prediction as shown by the dashed lines in the plot. All quantities are dimensionless (G_0 is the plateau modulus for G').

that our LB model is capable of predicting viscoelastic flow; see also fig. (1) and caption. We note that a dimensionless crossover point of $\omega\tau_r \sim 1$ consistently links rheological properties of the mixture with the relaxation time of the gyroid mesophase. This is encouraging for the use of this simulation model to inspect the correlation between macroscopic dynamics and mesoscopic structure. Indeed in the case of linear viscoelasticity, $G' \sim \omega^2$, $G'' \sim \omega$ as ω goes to 0 for any fluids. In fig. 5 we plot lines $\sim \omega$ and $\sim \omega^2$ as a guide for the eye; our data show excellent quantitative agreement with theory. We interpret the elastic response component as due to the stress response to mechanical perturbations of the long-range ordered equilibrium structure of the liquid gyroid crystalline mesophase. We also tried to fit the data in fig.5 to a simple single relaxation time (Maxwell) model of viscoelasticity but the fit is very poor. This suggests that there are several relaxation times present, as is to be expected here since the viscoelasticity arises from complex mesoscale structure. We note that the existence of a spectrum of relaxation times is consistent with the stretched-exponential behaviour of domain self-assembly in amphiphilic fluid systems found in [10].

Conclusions. – In this letter we use a purely kinetic LB model that leads to the emergence of non-trivial rheological properties. Non-Newtonian behaviour, in this case a decrease of viscosity with shear rate, has been shown for an initially self-assembled gyroid liquid crystalline mesophase. In addition, linear viscoelastic effects in the system are manifest in the simulations. It is notable that our model correctly predicts the theoretical limits for the moduli $G'(\omega)$, $G''(\omega)$ as ω goes to 0 as well as a crossover in $G'(\omega)$, $G''(\omega)$ at higher ω . We note that, unlike previous approaches, this model does not require any assumptions at the macroscopic level, that is it provides a purely kinetic-theoretical approach to the description of complex fluids. This model can therefore help in understanding complex flows, such as flow of viscoelastic liquids in porous media, colloidal fluids and polymer melts. Work is in progress to assess the generality of this approach within our lattice-Boltzmann model of amphiphilic fluids.

In particular, such simulations should enable us to investigate the link between mesoscopic structure and macroscopic dynamics, for example by correlating rheological relaxation times to mesoscale relaxation processes within the amphiphilic fluid.

* * *

We would like to thank D.M.A. Buzza for a critical reading of this manuscript, as well as J. Chin and N. González-Segredo for helpful discussions. This research is funded by EPSRC under the RealityGrid grant GR/R67699 which also provided access to UK national supercomputing facilities at CSAR and HCPx. Access to the US TeraGrid and Lemieux at Pittsburgh Supercomputing centre was provided through the National Science Foundation (USA) NRAC and PACS grants MCA04N014 and ASC030006P respectively. Intercontinental data transfer was effected via UKLight within EPSRC grant GR/T04465. G.G. would like to acknowledge the support of the European Commission's Research Infrastructure Activity, contract number 506079 (HPC Europa).

REFERENCES

- [1] S. Succi. *The Lattice Boltzmann Equation for Fluid Dynamics and Beyond*. Oxford University Press, 2001.
- [2] Y. H. Qian and Y. F. Deng. *Phys. Rev. Lett.*, 79(14):2742–2745, 1997.
- [3] I. Ispolatov and M. Grant. *Phys. Rev. E*, 65:056704, 2002.
- [4] L. Giraud, D. d'Humieres, and P. Lallemand. *Europhys. Lett.*, 42:625, 1998.
- [5] P. Lallemand, D. d'Humieres, L. Luo, and R. Rubinstein. *Phys. Rev. E*, 67:021203, 2003.
- [6] G. Pätzold and K. Dawson. *Phys. Rev. E*, 54:1669, 1996.
- [7] B. M. Boghosian, P. V. Coveney, and P. J. Love. *Phys. Rev. E*, 66:041401, 2002.
- [8] C. Denniston, E. Orlandini, and J. M. Yeomans. *Phys. Rev. E*, 63(056702), 2001.
- [9] V. M. Kendon, M. E. Cates, I. Pagonabarraga, J. C. Desplat, and P. Bladon. *J. Fluid Mech.*, 440:147–203, 2001.
- [10] N. González-Segredo and P. V. Coveney. *Phys. Rev. E*, 69:061501, 2004.
- [11] R. A. L. Jones. *Soft Condensed Matter*. Oxford University Press, 2003.
- [12] H. Chen, B. M. Boghosian, P. V. Coveney, and M. Nekovee. *Proc. R. Soc. Lond. A*, 456:2043–2047, 2000.
- [13] P. J. Higuera, S. Succi, and R. Benzi. *Europhys. Lett.*, 9(4):345–349, 1989.
- [14] P. L. Bhatnagar, E. P. Gross, and M. Krook. *Phys. Rev.*, 94(3):511–525, 1954.
- [15] S. Chen, H. Chen, D. Martínez, and W. Matthaeus. *Phys. Rev. Lett.*, 67(27):3776–3779, 1991.
- [16] X. Shan and H. Chen. *Phys. Rev. E*, 47(3):1815–1819, 1993.
- [17] X. Shan and H. Chen. *Phys. Rev. E*, 49(3):2941, 1994.
- [18] M. Nekovee, P. V. Coveney, H. Chen, and B. M. Boghosian. *Phys. Rev. E*, 62:8282, 2000.
- [19] J. Harting, J. Chin, M. Venturoli, and P. V. Coveney. *Phil. Trans. R. Soc. Lond. A*, 363:1895–1915, 2005.
- [20] N. Gonzalez-Segredo, J. Harting, G. Giupponi, and P. V. Coveney. Submitted (2005).
- [21] J. Harting, M. J. Harvey, J. Chin, and P. V. Coveney. *Comp. Phys. Comm.*, 165:97–109, 2004.
- [22] A. Lees and S. Edwards. *J. Phys. C.*, 5(15):1921–1928, 1972.
- [23] A. Wagner and I. Pagonabarraga. *J. Stat. Phys.*, 107:521, 2002.
- [24] M. E. Cates, J. C. Desplat, P. Stansell, A. J. Wagner, K. Stratford, R. Adhikari, and I. Pagonabarraga. *Phil. Trans. R. Soc. Lond. A*, 363:1917–1935, 2005.